

# Discovery of pulsations from NGC 300 ULX1 and its fast period evolution

S. Carpano,<sup>1\*</sup> F. Haberl,<sup>1</sup> C. Maitra,<sup>1</sup> G. Vasilopoulos<sup>1</sup>

<sup>1</sup>Max-Planck-Institut für extraterrestrische Physik, Giessenbachstraße 1, 85748 Garching, Germany

Accepted XXX. Received YYY; in original form ZZZ

## ABSTRACT

The supernova impostor SN 2010da located in the nearby galaxy NGC 300, later identified as a likely supergiant B[e] high-mass X-ray binary, was simultaneously observed by *NuSTAR* and *XMM-Newton* between 2016 December 16 and 20, over a total time span of  $\sim 310$  ks. We report the discovery of a strong periodic modulation in the X-ray flux with a pulse period of 31.6 s and a very rapid spin-up, and confirm therefore that the compact object is a neutron star. We find that the spin period is changing from 31.71 s to 31.54 s over that period, with a spin-up rate of  $-5.56 \times 10^{-7} \text{ s s}^{-1}$ , likely the largest ever observed from an accreting neutron star. The spectrum is described by a power-law and a disk black-body model, leading to a 0.3–30 keV unabsorbed luminosity of  $4.7 \times 10^{39} \text{ erg s}^{-1}$ . Applying our best-fit model successfully to the spectra of an *XMM-Newton* observation from 2010, suggests that the lower fluxes of NGC 300 ULX1 reported from observations around that time are caused by a large amount of absorption, while the intrinsic luminosity was similar as seen in 2016. A more constant luminosity level is also consistent with the long-term pulse period evolution approaching an equilibrium value asymptotically. We conclude that the source is another candidate for the new class of ultraluminous X-ray pulsars.

**Key words:** stars: neutron – pulsars: individual: NGC 300 ULX1 – galaxies: individual: NGC 300 – X-rays: binaries

## 1 INTRODUCTION

NGC 300 is a nearby, face-on spiral galaxy located in the Sculptor galaxy group at a distance of 1.88 Mpc (Gieren et al. 2005). The X-ray source population of the galaxy was first studied using ROSAT data (Read & Pietsch 2001) and later with *XMM-Newton* (Carpano et al. 2005). So far the brightest, but persistent, X-ray source was the Wolf-Rayet/black hole X-ray binary NGC 300 X-1, with a luminosity of  $\sim 2 \times 10^{38} \text{ erg s}^{-1}$  (Carpano et al. 2007). In May 2010 a new bright source appeared in NGC 300, at optical wavelengths, that was originally classified as a supernova (Monard 2010). The source was also detected by *Swift* XRT with an unabsorbed luminosity of  $6 \times 10^{38} \text{ erg s}^{-1}$  (Immler et al. 2010). Four months later, SN 2010da was detected at  $\sim 7\sigma$  significance by *Chandra* ACIS-I at coordinates  $\alpha_{J2000} = 00^{\text{h}}55^{\text{m}}04^{\text{s}}.85$  and  $\delta_{J2000} = -37^{\circ}41'43''.5$  with a 0.3–10 keV unabsorbed luminosity of  $\sim 2 \times 10^{37} \text{ erg s}^{-1}$  (Binder et al. 2011). From the high X-ray luminosity associated to the large optical/IR flare, the authors conclude that the system is a high-mass X-ray binary (HMXB) system in outburst. More recent *Chandra* observations of the source were

carried out in May and November 2014, when the luminosity changed by a factor of  $\sim 10$ , going from  $\sim 4 \times 10^{36} \text{ erg s}^{-1}$  to  $\sim 4 \times 10^{37} \text{ erg s}^{-1}$  (Binder et al. 2016), which is much less than what was observed during the 2010 outburst. Using spectroscopic and photometric data performed in the UV to infrared wavelengths, the source has been later reinterpreted as a supergiant B[e] HMXB (Lau et al. 2016; Villar et al. 2016).

Ultraluminous X-ray sources (ULXs; for a review see Kaaret et al. 2017) are off-nuclear point-like X-ray sources exceeding the (isotropic) Eddington limit for a neutron star or stellar-mass black hole, which is  $1.3 \times 10^{38} (M/M_{\odot}) \text{ erg s}^{-1}$ . For a  $1.4 M_{\odot}$  neutron star, the Eddington limit (bolometric luminosity) is  $\sim 2 \times 10^{38} \text{ erg s}^{-1}$ . Several pulsating ultraluminous X-ray sources (ULPs) have been discovered in nearby galaxies, the brightest ones being M82 X-2, NGC 7793 P13 and NGC 5907 ULX1. M82 X-2 was discovered with *NuSTAR* having an average pulse period of 1.37 s with a 2.5 d sinusoidal modulation, and a 3–30 keV luminosity of  $4.9 \times 10^{39} \text{ erg s}^{-1}$  (Bachetti et al. 2014). The period derivative  $\dot{P} = -2 \times 10^{-10} \text{ s s}^{-1}$  was calculated over a time interval of 5 days. The second bright ULP, NGC 7793 P13 has a pulse period of 0.42 s discovered with *XMM-Newton* and *NuSTAR* in May 2016 with a peak luminosity of  $\sim 10^{40}$

\* E-mail: scarpano@mpe.mpg.de

erg s<sup>-1</sup> and a  $\dot{P} = -3.5 \times 10^{-11} \text{ s s}^{-1}$  measured over a time span of three years (Fürst et al. 2016; Israel et al. 2017b). The third very bright ULP, NGC 5907 ULX1 with a bolometric luminosity reaching 10<sup>41</sup> erg s<sup>-1</sup>, was discovered with a pulse period of 1.1 s, a  $\dot{P} = -8 \times 10^{-10} \text{ s s}^{-1}$  and a probable orbital modulation of 5.3 d (Israel et al. 2017a). Several other super-Eddington pulsating sources have been reported in the literature, one of these being CXOU J073709.1+653544, in NGC 2403, which is one of the fastest spin-up ULPs with a  $\dot{P} = -1.1 \times 10^{-7} \text{ s s}^{-1}$  with a pulse period of  $\sim 18$  s (Trudolyubov et al. 2007).

In this letter, we report the discovery of the pulse period of the supernova impostor SN 2010da, hereafter referred as NGC 300 ULX1, observed in a very long *XMM-Newton* observation performed simultaneously to *NuSTAR* in December 2016. The discovery was already announced via the ATel#11158 (Carpano et al. 2018). The first section describes the *XMM-Newton* and *NuSTAR* observation and data reduction. We then explain in Sec. 3 our analysis of the pulse period and the period derivative. A spectral analysis of the source is performed in Sec. 4. Conclusions are ending the paper.

## 2 OBSERVATIONS AND DATA REDUCTION

NGC 300 ULX1 was visible in three *XMM-Newton* (Jansen et al. 2001) observations: 0656780401 performed on 2010 May 28 for a duration of 18 ks when the source was observed in outburst for the first time, and two consecutive observations, 0791010101 and 0791010301, performed from 2016 December 17 to 20, for a duration of 139+82 ks. The data were reduced following standard procedures using the *XMM-Newton* SAS data analysis software version 16.1.0 with the calibration files (CCFs) available in January 2018. For the source extraction region we used a circle around the *Chandra* coordinates mentioned in Sec. 1 with a radius of 40". The background region was centred on a region equidistant from the source extraction region to the nearby source NGC 300 X-1, in order to minimise possible contamination after background subtraction. It was centred on  $\alpha_{J2000} = 00^{\text{h}}55^{\text{m}}07^{\text{s}}.50$  and  $\delta_{J2000} = -37^{\circ}43'15''.3$  with a radius of 40". For the spectral analysis, periods of flaring background were removed from the data by removing the time intervals with background rates  $\geq 8$  and 2.5 cts ks<sup>-1</sup> arcmin<sup>-2</sup> for EPIC-pn and EPIC-MOS respectively (Sturm et al. 2013). Event extraction was performed using the SAS task `evselect` applying the standard filtering criteria (`#XMMEA_EP && PATTERN<=4` for EPIC-pn and `#XMMEA_EM && PATTERN<=12` for EPIC-MOS).

The source was observed for the first time with *NuSTAR* (Harrison et al. 2010) on 2016 December 16, for an exposure time of 163 ks. The data were processed using the *NuSTAR*-DAS software version 1.8.0 (released with HEASOFT v.6.22.1) and calibration files (CALDB) version 20171002, while the spectra, response files and barycenter-corrected event files were produced using the `nuproducts` task. The source and background extraction regions are a circle and annulus, respectively, both centred on the *Chandra* coordinates (since NGC 300 X-1 was not visible in the data), with a radius of 50" for the source and radii of 60" and 100" for the background.

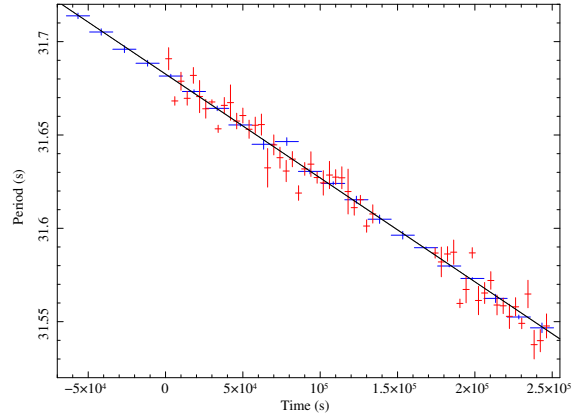


**Figure 1.** Spin period evolution of NGC 300 ULX1 obtained from 4 ks intervals of EPIC-pn (red crosses) and 15 ks intervals of *NuSTAR* data (blue crosses). The straight line represents the best-fit model of a linear period decrease applied to both data sets. Time zero corresponds to the start of the EPIC-pn exposure.

## 3 PULSE PERIOD AND ITS EVOLUTION

To refine the spin period evolution reported from NGC 300 ULX1 (Carpano et al. 2018), we used a Bayesian method which uses an epoch-folding algorithm to calculate frequency-dependent odds-ratios, which describe how the data favour a periodic model over the unpulsed model for a given frequency (Gregory & Loredo 1996; Haberl et al. 2008). The analysis of the peak in the odds-ratio periodogram provides the most probable frequency and the 1 $\sigma$  uncertainty.

To investigate the period evolution during the *XMM-Newton*/*NuSTAR* observations we split the EPIC-pn data, which provides the best statistics with high time resolution (73 ms), into 4 ks intervals. The arrival times of the events from the source region (in the 0.2–10 keV band) were then analysed for all 53 intervals from the two observations. For *NuSTAR* we combined the data from the two instruments, used 21 intervals of 15 ks and an energy band of 3–20 keV. The inferred evolution of the spin period is shown in Fig. 1. The spin period of NGC 300 ULX1 decreased linearly from  $\sim 31.71$  s at the start of the *NuSTAR* observation to  $\sim 31.54$  s at the end of the *XMM-Newton*/*NuSTAR* observations. The period derivative inferred from a model with a constant and linear term fitted to the *XMM-Newton* and *NuSTAR* data is  $(-5.563 \pm 0.024) \times 10^{-7} \text{ s s}^{-1}$  with a spin period of  $31.68262 \pm 0.00036$  s at the start of the of the EPIC-pn exposure (MJD 57739.39755). We note that the introduction of an additional sine function to fit the period evolution seen from EPIC-pn as reported in Carpano et al. (2018) was caused by a software problem. In our refined analysis, we didn't find any significant deviation from a linear model and derive an upper limit for  $v \cdot \sin(i)$  of  $\sim 4.6 \times 10^{-5} c$  (assuming orbital periods between one and three days), which translates into upper limits for the mass function of  $\sim 8 \times 10^{-4} M_{\odot}$  and for the inclination of  $\sim 3^{\circ}$  for a  $20 M_{\odot}$  companion star.

Taking into account the constant value for  $\dot{P}$  derived above, we converted the arrival times to spin phase ( $\phi = \phi_0 + (t - t_0) \times f + 0.5(t - t_0)^2 \times \dot{f}$ ). The pulse profiles (phase histogram) for the first *XMM-Newton* and the *NuSTAR* observation are shown in Fig. 2. The pulsed fraction (0.2–10 keV), defined as proportion of flux integrated over the pulse profile

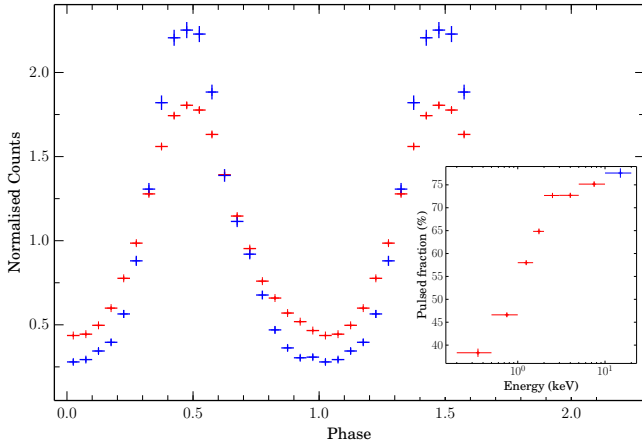


**Figure 2.** Pulse profile of NGC 300 ULX1 obtained from the 0.2–10 keV EPIC-pn data of the first 2016 observation (red), and the 3–20 keV light curve from the combined NuSTAR instruments (blue). Both profiles are background subtracted and corrected for the pulsar spin-up. The inset shows the pulsed fraction as function of energy with colours as in the main plot.

above minimum flux relative to the total integrated flux, increased slightly from  $56.3 \pm 0.3\%$  during the first 2016 *XMM-Newton* observation to  $57.4 \pm 0.3\%$  in the second. The pulsed fraction also increases strongly with energy with  $72.1 \pm 0.4\%$  in the *NuSTAR* data (3–20 keV).

#### 4 SPECTRAL ANALYSIS

X-ray spectral analysis was performed using XSPEC version 12.9.1 (Arnaud 1996). To account for the interstellar absorption, the model *TBabs* was used, with abundances from Wilms et al. (2000). In order to investigate the broad-band X-ray spectrum of NGC 300 ULX1, we fitted the spectra from the overlapping 2016 *XMM-Newton* and *NuSTAR* observations simultaneously. Spectra from all the EPIC cameras and *NuSTAR* focal plane modules (FPMA and FPMB) were fitted together with a constant multiplicative factor accounting for inter-calibration uncertainties and an intensity change between the *XMM-Newton* observations (with respect to EPIC-pn of 0791010101). The *NuSTAR* spectral analysis was limited at high energies to 30 keV due to the background dominating the spectrum above this energy.

We started fitting the spectra with a two-component model consisting of a power law with high-energy cutoff and a soft thermal component (disk black-body). Similar models have been successfully used to model the spectra of ULXs hosting neutron stars (Israel et al. 2017b; Pintore et al. 2017). However, the resultant fit to the spectra of NGC 300 ULX1 was unsatisfactory, with residuals visible at energies  $< 0.5$  keV. The residuals indicate the presence of a further softer spectral component which can be attributed to the scattering and reprocessing of the X-ray photons originating in the vicinity of the neutron star, by an additional absorber. This was modelled using a partial-covering absorber component. Further addition of this partial absorber component to the power law alone did not improve the fit. However, the fit improved significantly ( $\Delta\chi^2 = 20$ ) and was

**Table 1.** Simultaneous fit of the 2016 *XMM-Newton* and *NuSTAR* spectra. Errors are quoted at the 90% confidence.

Component	Parameter	Value
TBabs	$N_H$ <sup>a</sup>	$0.11 \pm 0.01$
Pcfabs	$N_H$ <sup>a</sup>	$0.75 \pm 0.07$
Power law	$cv_{frac}$	$0.85 \pm 0.03$
	$\Gamma$	$1.52 \pm 0.03$
	Ecut (keV)	$5.6 \pm 0.2$
	Efold (keV)	$7.0 \pm 0.3$
Disk black-body	$F_x$ <sup>b</sup>	$6.4 \pm 0.1$
	$kT$ (keV)	$0.178^{+0.008}_{-0.007}$
	$F_x$ <sup>b</sup>	$4.4 \pm 0.1$
$L_x$ <sup>c</sup>		4.7
$\chi^2_{red}/d.o.f.$		1.13/1167

Spectral model used in XSPEC convention:

$$TBabs<1>*pcfabs<2>(powerlaw<3>*highcut<4> + diskbb<5>+gaussian<6>)$$

The obtained values of the normalisation constants for EPIC-MOS1 and MOS2 were  $0.98 \pm 0.01$  and  $0.98 \pm 0.01$  for 0791010101, and  $1.01 \pm 0.02$  and  $0.99 \pm 0.01$  for 0791010301, respectively. The corresponding values for EPIC-pn for 0791010301 and *NuSTAR* FPMA and FPMB were  $1.05 \pm 0.01$ ,  $0.86 \pm 0.02$  and  $0.86 \pm 0.02$ , respectively.

<sup>a</sup> in  $10^{22}$  atoms  $\text{cm}^{-2}$

<sup>b</sup> Unabsorbed flux (0.3–30 keV) in  $10^{-12}$  erg  $\text{cm}^{-2}$   $\text{s}^{-1}$

<sup>c</sup> Unabsorbed luminosity (0.3–30 keV) in  $10^{39}$  erg  $\text{s}^{-1}$

satisfactory when the partial absorber was applied to the power-law and black-body components together. This can be understood if the underlying continuum consists of a combination of power-law component (originating from the vicinity of the neutron star) plus a disk black-body component (originating from the inner accretion disk), modified by scattering and absorption by additional material. **This is most likely located in the clumpy wind of the supergiant companion or inner part of the circum-stellar disk of a Be star.** The reduced  $\chi^2$  of the fit is 1.13 for 1167 degrees of freedom. The spectra and the best-fit model are shown in Fig. 3 (top) and the spectral model with the best-fit parameters is summarised in Table. 1.

The *XMM-Newton* spectrum taken in 2010 is drastically different compared to that in 2016, with a soft component seen at energies  $< 2$  keV, **an almost flat spectrum between 2–4 keV and a bump-like feature above 5 keV. This can be explained if the column density was significantly higher in 2010 and the direct component of the emission was reduced drastically.** A similar approach was adopted by Coe et al. (2015) to explain the change in the spectrum of the Be/X-ray binary pulsar SXP 5.05. To investigate this, we fitted the EPIC-pn spectra of the three observations simultaneously assuming the same underlying continuum spectrum as used in the broad-band spectral fit, and allowing only certain parameters to vary. Apart from varying all the absorption components, the power-law normalisation was left to vary in order to account for an intrinsic variation in the X-ray luminosity of the source. The resultant fit is satisfactory with a reduced  $\chi^2$  of 1.06 for 345 degrees of freedom. The spectra and the best-fit model are shown in Fig. 3 (bottom) and the spectral model with the best-fit parameters is summarised in Table. 2. **The change in the 2010 *XMM-Newton* spectra**

**Table 2.** Results of the simultaneous fit to the EPIC-pn spectra from the 2016 and 2010 observations.

Observation	0791010101	0791010301	0656780401
$N_{\text{H,TBabs}}(10^{22})$	$0.11 \pm 0.02$	$0.11^b$	$0.61^{+0.17}_{-0.12}$
$N_{\text{H,Pcfabs}}(10^{22})$	$0.66 \pm 0.10$	$0.66^b$	$47.2 \pm 15.3$
$cv_{\text{frac}}$	$0.84 \pm 0.04$	$0.84^b$	$0.95 \pm 0.02$
$\Gamma$	$1.54 \pm 0.04$	$1.54^a$	$1.54^a$
Ecut (keV)	$6.6 \pm 0.3$	$6.6^a$	$6.6^a$
Efold (keV)	$4.8^{+1.2}_{-0.8}$	$4.8^a$	$4.8^a$
$F_{\text{x,pl}}^c$	$5.62 \pm 0.01$	$6.02 \pm 0.01$	$2.50 \pm 0.14$
$kT$ (keV)	$0.17 \pm 0.01$	$0.17^a$	$0.17^a$
$F_{\text{x,bbbody}}^c$	$5.60 \pm 0.16$	$5.60^a$	$5.60^a$
$L_{\text{x,total}}^c$	4.2	4.4	2.8
$\chi^2_{\text{red}}/\text{d.o.f.}$		1.06/345	

(a) parameters of the underlying continuum were linked to the parameters obtained from observation 0791010101.

(b) The absorber components of the 2016 *XMM-Newton* observations were linked as no significant variation was seen.

(c) Units for the unabsorbed flux and luminosity are as in Table 1, but in the energy range of 0.3–10 keV.

can be explained by a large increase in the column density of both absorption components and the direct component of the underlying continuum reduced to a mere 5%. This model predicts an absorption corrected intrinsic luminosity of  $2.8 \times 10^{39} \text{ erg s}^{-1}$  which is not very different from the luminosity estimates from the 2016 observations (Table 2). An Fe-K $\alpha$  fluorescence line was noticed in the spectrum of the 2010 *XMM-Newton* observation as expected in the case of reprocessed emission. The line energy is  $6.40^{+0.14}_{-0.07} \text{ keV}$  and the equivalent width is  $348 \pm 93 \text{ eV}$ . No line was required to fit the spectra of the 2016 observations as the continuum completely dominates at this energy range.

## 5 DISCUSSION AND CONCLUSIONS

We report the discovery of pulsations from NGC 300 ULX1 with a period of  $\sim 31.6 \text{ s}$  and strong spin-up during simultaneous *XMM-Newton*/*NuSTAR* observations. To our knowledge, the secular spin period derivative of  $-5.56 \times 10^{-7} \text{ s s}^{-1}$  seen over three days is the highest ever observed from an accreting neutron star. The analysis of archival *Swift* observations has shown that the strong spin-up seen during the *XMM-Newton*/*NuSTAR* observations lasts already for at least 21 months (Vasilopoulos et al. 2018; Grebenev & Mereminskiy 2018; Kennea 2018). The period history as shown in Fig. 4 follows an exponential decrease with e-folding time of  $\sim 1.5$  years, approaching an equilibrium value asymptotically. A fit using a model with constant plus exponential function yields values between 8.5 s and 14 s, depending on the consideration of all measurements or only *XMM-Newton*/*NuSTAR* and later, respectively.

The extreme spin-up of the pulsar with luminosity seen over the duration of the *XMM-Newton*/*NuSTAR* observations can be used to constrain the magnetic field strength (B) of the neutron star. Using the standard disk accretion model of Ghosh & Lamb (1979), B can be estimated from the derived spin period,  $\dot{P}$  and the luminosity estimated from

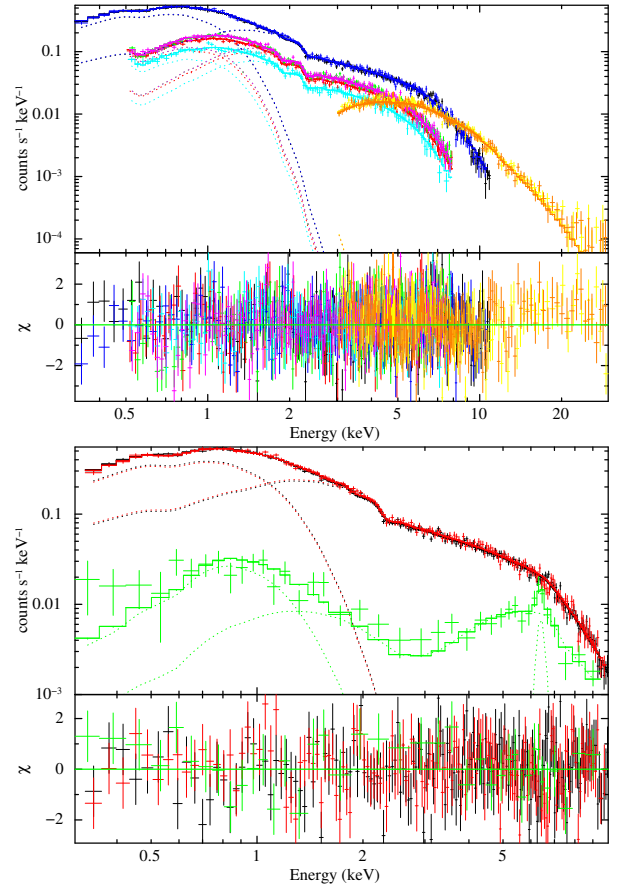


**Figure 3.** The top panels show the simultaneous broad-band spectral fit of NGC 300 ULX1 using the 2016 *XMM-Newton* and *NuSTAR* spectra from all the *XMM-Newton*/EPIC cameras (pn in black and blue, MOS in red, green, magenta and cyan) and *NuSTAR* focal plane modules (FPMA and FPMB in yellow and orange), along with the best-fit model (upper panel). The panel underneath displays the residuals for the best-fit model. The bottom panels show the simultaneous spectral fit of NGC 300 ULX1 using the EPIC-pn spectra together with the residuals as above. Observation 0791010101 is marked in black, 0791010301 in red and 0656780401 (from 2010) in green.

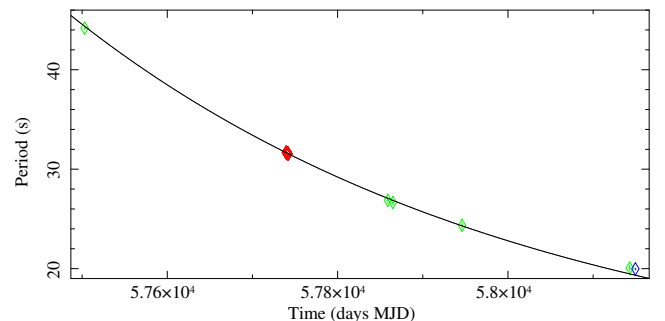


**Figure 4.** Long-term time evolution of the pulse period of NGC 300 ULX1 from 2016-04-25 to 2018-02-01. The simultaneous *XMM-Newton*/*NuSTAR* observation is marked in red, *Swift* in green and the recent *NuSTAR* observation (Bachetti et al. 2018) in blue. To account for multiple solutions in the short *Swift* observations we use a  $\pm 0.3 \text{ s}$  error which includes aliasing effects due to the *Swift* satellite orbit.



the *XMM-Newton*/*NuSTAR* observations. The dimensionless accretion torque  $\eta(\omega)$  is estimated using the analytic expression from Ghosh & Lamb (1979) which is accurate up to 5% and is valid in our regime ( $0 < \eta(\omega) < 0.9$ ). The estimated  $B$  is  $\sim 3 \times 10^{12}$  G. On the other hand the equilibrium spin period of  $\sim 8.5$ – $14$  s derived from Fig. 4 can also be used to estimate  $B$ , for a given average luminosity (see Ho et al. 2014). Assuming an average luminosity of  $2 \times 10^{39}$  erg s $^{-1}$   $B$  is  $\sim 1 \times 10^{13}$  and  $\sim 2 \times 10^{13}$  G, assuming equilibrium spin period of 8.5 and 14 s respectively. Although the estimate of  $B$  from the standard accretion torque theory is lower than that predicted from the equilibrium spin period, the difference can be bridged by a considerable extent by accounting for a higher accretion efficiency than obtained by considering the gravitational potential for a neutron star of standard mass ( $1.4 M_{\odot}$ ) and radius (10 km). In any case these estimates need to be handled with caution as the model assumptions (geometrically thin disk and sub-Eddington accretion) are not fulfilled in the extreme case of NGC 300 ULX1.

The average pulsed fraction seen from NGC 300 ULX1 of around 55% in the *XMM-Newton* energy band 0.2–10 keV and 72% in the *NuSTAR* band 3–20 keV is higher than for the other known ULPs: for NGC 7793 P13 it increases from  $\sim 10\%$  to  $\sim 40\%$  in the *XMM-Newton* band (Israel et al. 2017b), for NGC 5907 ULX1 it grows from  $\sim 12\%$  to  $\sim 20\%$  (Israel et al. 2017a, *XMM-Newton* band), and M82 X-2 also shows the highest pulsed fraction of  $\sim 23\%$  at higher energies (Bachetti et al. 2014, 10–30 keV). The pulsed fraction for NGC 300 ULX1 rises strongly from  $\sim 37\%$  (0.2–0.5 keV) to  $\sim 70\%$  around 2 keV. Above 2 keV the rise is flatter reaching nearly 80% in the 10–20 keV band. This suggests that the soft black-body like emission component is not pulsed and does not originate at the neutron star surface. A likely origin is the accretion disk.

Our analysis of the X-ray spectra obtained by *XMM-Newton* and *NuSTAR* in Dec. 2016 shows that they can be represented by a two-component model with a dominating power law (photon index  $\sim 1.6$  and soft black-body emission (kT  $\sim 0.18$  keV). A high-energy cutoff around 6.6 keV is similar as seen from other ULXs (Gladstone et al. 2009). Our model is also similar to what is observed from supergiant HMXBs, although the power law is quite steep and the high-energy cutoff starts at a relatively low energy.

The archival *XMM-Newton* spectrum from 2010 can be modelled by the same continuum, however requires a much higher absorption. This indicates that NGC 300 ULX1 was also in the ULX state at similar intrinsic X-ray luminosity, albeit highly absorbed in 2010. It is to be noted that the *Chandra* spectra of NGC 300 ULX1 from 2010 and 2014 exhibited a spectrum very similar to that observed with *XMM-Newton* in 2010 (Binder et al. 2011, 2016). The fact that we see a strong fluorescent Fe line in 2010, but not in 2016 is also consistent with the picture of very different absorption in these two epochs. Statistical limitations of the earlier data inhibited a detailed spectral modelling in previous works. However, accounting for a highly absorbed continuum emission similar to that demonstrated in this paper can result in a much higher intrinsic luminosity than quoted in earlier publications. The high absorption during the first years after the supernova impostor event suggests that a large amount of material was expelled during the event which expanded and became now transparent to soft X-rays.

## ACKNOWLEDGEMENTS

This research has made use of data obtained with *XMM-Newton*, an ESA science mission with instruments and contributions directly funded by ESA Member States and NASA, and data obtained from the *NuSTAR* Data Archive. The *XMM-Newton* project is supported by the Bundesministerium für Wirtschaft und Technologie/Deutsches Zentrum für Luft- und Raumfahrt (BMWi/DLR, FKZ 50OG1601) and the Max Planck Society.

## REFERENCES

- Arnaud K. A., 1996, in Jacoby G. H., Barnes J., eds, A. S. P. Conference Series Vol. 101, A. D. A. S. S. V. p. 17
- Bachetti M., et al., 2014, *Nature*, **514**, 202
- Bachetti M., Grefenstette B. W., Walton D. J. W., et al., 2018, The Astronomer’s Telegram, 11282
- Binder B., Williams B. F., Kong A. K. H., Gaetz T. J., Plucinsky P. P., Dalcanton J. J., Weisz D. R., 2011, *ApJ*, **739**, L51
- Binder B., Williams B. F., Kong A. K. H., Gaetz T. J., Plucinsky P. P., Skillman E. D., Dolphin A., 2016, *MNRAS*, **457**, 1636
- Carpano S., Wilms J., Schirmer M., Kendziorra E., 2005, *A&A*, **443**, 103
- Carpano S., Pollock A. M. T., Wilms J., Ehle M., Schirmer M., 2007, *A&A*, **461**, L9
- Carpano S., Haberl F., Maitra C., 2018, The Astronomer’s Telegram, 11158
- Coe M. J., Bartlett E. S., Bird A. J., Haberl F., et al., 2015, *MNRAS*, **447**, 2387
- Fürst F., et al., 2016, *ApJ*, **831**, L14
- Ghosh P., Lamb F. K., 1979, *ApJ*, **234**, 296
- Gieren W., Pietrzyński G., Soszyński I., Bresolin F., Kudritzki R.-P., Minniti D., Storm J., 2005, *ApJ*, **628**, 695
- Gladstone J. C., Roberts T. P., Done C., 2009, *MNRAS*, **397**, 1836
- Grebenev S. A., Mereminskiy I. A., 2018, The Astronomer’s Telegram, 11228
- Gregory P. C., Lored T. J., 1996, *ApJ*, **473**, 1059
- Haberl F., Eger P., Pietsch W., 2008, *A&A*, **489**, 327
- Harrison F. A., et al., 2010, in Space Telescopes and Instrumentation 2010: Ultraviolet to Gamma Ray. p. 77320S
- Ho W. C. G., Klus H., Coe M. J., Andersson N., 2014, *MNRAS*, **437**, 3664
- Immler S., Brown P., Russell B. R., 2010, The Astronomer’s Telegram, 2639
- Israel G. L., et al., 2017a, *Science*, **355**, 817
- Israel G. L., et al., 2017b, *MNRAS*, **466**, L48
- Jansen F., et al., 2001, *A&A*, **365**, L1
- Kaaret P., Feng H., Roberts T. P., 2017, *ARA&A*, **55**, 303
- Kennea J. A., 2018, The Astronomer’s Telegram, 11229
- Lau R. M., et al., 2016, *ApJ*, **830**, 142
- Monard L. A. G., 2010, Central Bureau Electronic Telegrams, 2289
- Pintore F., Zampieri L., Stella L., Wolter A., Mereghetti S., Israel G. L., 2017, *ApJ*, **836**, 113
- Read A. M., Pietsch W., 2001, *A&A*, **373**, 473
- Sturm R., et al., 2013, *A&A*, **558**, A3
- Trudolyubov S. P., Priedhorsky W. C., Córdova F. A., 2007, *ApJ*, **663**, 487
- Vasilopoulos G., Haberl F., Carpano S., Maitra C., 2018, The Astronomer’s Telegram, 11179
- Villar V. A., et al., 2016, *ApJ*, **830**, 11
- Wilms J., Allen A., McCray R., 2000, *ApJ*, **542**, 914